Electron pair production from pulsed electromagnetic fields in relativistic heavy-ion collisions

C. Bottcher and M. R. Strayer
Physics Division, Oak Ridge National Laboratory, Oak Ridge, Tennessee 37831
(Received 6 September 1988)

We present calculations of the electron pair production cross sections in relativistic heavy-ion collisions. The electron pairs arise from the decay of vacuum excitations induced by the very strong and sharply pulsed electromagnetic fields near nuclei which collide at relativistic velocities. We present an exact Monte Carlo evaluation of the two-photon terms describing this process, and we discuss at length the inadequacies of the approximation schemes that are inherent to the usual virtual-photon approaches. Typical results for collisions corresponding to experiments at the BNL Alternating Gradient Synchrotron, CERN, and the Relativistic Heavy Ion Collider are discussed.

I. INTRODUCTION

One of the most useful modern probes of hadronic matter is the associated production and decay of lepton pairs during a collision.[1] In such collisions, lepton-hadron final-state interactions are usually small, and hence the leptons carry direct information on the space-time region of creation. Historically, lepton pair production has been an important tool in collider experiments, in part, because the special relationship between deep-inelastic lepton-hadron scattering and the large-mass Drell-Yan processes provide complementary information on quantum chromodynamics (QCD) in the asymptotic regime.[2,3] From these experiments have arisen new ideas and phenomena: scaling, chiral, and flavor symmetry, charm, and a quantitative understanding of a rich meson and baryon spectroscopy.[4,5]

In ultrarelativistic heavy-ion collisions, lepton pair processes have been widely discussed as a possible tool to help probe the formation and the decay of the quark-gluon-plasma phase of matter.[6,7] Although lepton-pair-production measurements are sensitive probes of the local space-time region where they are formed, the detailed behavior of the deconfining phase transition with the subsequent expansion and rehadronization strongly affects the lepton yields. No clearly identifiable signal has emerged from these studies that will diagnose the formation of the plasma.[8,9] In contrast with the high-mass Drell-Yan pairs studied in high-energy proton and electron collider experiments, the dilepton signals from the relativistic heavy-ion collisions are not asymptotically free, and are strongly dependent on the nonlinear structure of QCD (Ref. 10).

It has been suggested by several authors[11–13] that other sources of lepton pairs might possibly mask the signals from the plasma phase. In such collisions, the near-zone electromagnetic fields associated with the colliding ions can readily produce large numbers of lepton pairs.[14,15] The present work addresses a series of questions that arise in attempting to calculate the electron pair production cross sections from such strong fields. In studying the production of high-mass electron-positron pairs, the long-range electromagnetic production is usually treated with perturbative methods.[16–19] Particular approximations based on Refs. 18 and 19 have been extensively applied as either the equivalent-photon or the Weizsäcker-Williams method.[20–26] In this method it is usually assumed that the lowest nonzero terms in the perturbation series are the diagrams with two intermediate photons, and that these terms suffice to describe the electromagnetic production phenomena.[26] There are also additional assumptions: the photons must be on shell, the corresponding S matrix elements, which are singular, are regularized with both high- and low-frequency cutoffs, the source currents must either correspond to the motion of point charges, or be excluded from the volume containing the pairs. Only incoherent pair production can be calculated with the method. A derivation of the method with a good discussion of these points is given in Ref. 27.

In the context of the ultrarelativistic collisions of two nuclei, different assumptions on the electromagnetic structure of the constituent nucleons yield very different results for the pair production: if we assume nucleons are comprised of valence quarks and sea-quark–antiquark pairs, then single-photon-exchange mechanisms, which are approximately proportional to $Z\alpha$, also contribute to the pair production; otherwise the lowest-order terms are the two-photon-exchange diagrams which are proportional to $(Z\alpha)$ (Ref. 28). The yield from these two processes is quite different. Also, since $Z\alpha$ is not small, and since very large fields develop during the collision, the production of pairs from processes containing many exchanged photons gives rise to the coherent production of pairs. The coherent production of photons from such collisions has been discussed,[29] and it is worth noting that the photon multiplicity and the details of the spectrum are sensitive to both low- and high-frequency cutoffs. Similar cutoffs are necessary to regularize the electron production in the two-photon diagrams.

In the present paper, we depart from previously mentioned work in several respects. We assume that fields from the heavy ions can be represented by prescribed

 ©1989 The American Physical Society

time-dependent classical fields. This is briefly discussed in Sec. II, together with a treatment of the formalism. Our study of the electromagnetic production via two-photon processes is presented in Sec. III, with details of the method and gauge invariance in the Appendixes. We work in the center-of-momentum frame of the colliding nuclei. For the two-photon diagrams, this makes transparent the essential symmetries and the large cancellation in the amplitude for low-momentum pairs.[30] In this section, our discussion is principally focused on a theoretical analysis and the evaluation of the two-photon diagrams using Monte Carlo integration; we consider such points as the violation of unitarity and high-energy bounds on total cross sections.[32,31] In Sec. IV typical results for collisions which represent experiments at the BNL Alternating Gradient Synchrotron (AGS), CERN, and at the Relativistic Heavy Ion Collider (RHIC) are presented and compared to those obtained with approximate methods. Finally, we summarize our results and conclusions.

II. FORMALISM

We propose to treat the production of electron pairs using a semiclassical formalism, wherein the electron states evolve in the presence of classical electromagnetic potentials. The source currents for the potentials are the Lorentz-boosted charge distributions of the two heavy ions. For the present purposes of exposition, it is most convenient to consider the symmetric collision of two heavy nuclei in the center-of-momentum (c.m.) frame. In the case of structureless point charge nuclei, these potentials are the retarded Liénard-Wiechert interactions.[33] The realistic calculation of electron pair production requires a detailed knowledge of the charge currents of nucleons within each nucleus, and also the charge structure functions of the individual nucleons. Although a fully dynamical understanding of such currents in terms of a fundamental theory such as QCD is presently not possible, models for incorporating these effects into the calculations are well known,[34] and they will be treated in future work.

We develop the equations governing pair production in the spirit of Schwinger's space-time picture of electrodynamics,[35] with appropriate modifications to allow for the classical motion of the heavy ions. The two important differences are the localization of the fields along an impact parameter transverse to the motion of the ions, and the large number of virtual photons in the fields. The semiclassical coupling of electrons to the electromagnetic field is given by the Lagrangian density[36]

$$\mathcal{L}_{\rm int}(x)=-\bar{\Psi}(x)\gamma_\mu\Psi(x)A^\mu(x)\ , \tag{1}$$

which separately conserves electron number,[12] and only depends on the field variables via the classical four-potential A^μ. Given the Lagrangian (1), the equations of motion for state vectors in the Schrödinger picture follow from three basic assumptions.

(i) We construct a semiclassical action in terms of a time-dependent *many-electron* state $\Phi(t)$:

$$\mathcal{S}=\int d^4x\,\langle\Phi(t)|:\mathcal{L}_0(x)+\mathcal{L}_{\rm int}(x):|\Phi(t)\rangle\ , \tag{2}$$

where the normal ordering is with respect to an unspecified reference state and where $\mathcal{L}_0$ is the usual noninteracting fermion Lagrangian

$$\mathcal{L}_0(x)=\bar{\Psi}(x)(\gamma_\mu i\partial^\mu-m)\Psi(x)\ . \tag{3}$$

In (2), the dynamical coordinates which are varied to make the action stationary are the parameters labeling the state vector $\Phi(t)$ and not the field operators.

(ii) We assume that the initial state vector corresponds to a single Slater determinant, $|0\rangle$,

$$\lim_{t\to-\infty}|\Phi(t)>\to|0\rangle\ . \tag{4}$$

Since we shall only consider pair production out of the vacuum, we choose $|0\rangle$ as the vacuum state, which we also identify as the reference state for the ordering in (2). By construction, we have a well-defined initial Hamiltonian with a corresponding complete and orthonormal set of single-particle states:

$$\begin{aligned}&\sum_q|\chi_q^{(+)}\rangle\langle\chi_q^{(+)}|+|\chi_q^{(-)}\rangle\langle\chi_q^{(-)}|=1\ ,\\&\langle\chi_q^{(i)}|\chi_p^{(j)}\rangle=\delta_{q,p}\delta_{i,j}\ .\end{aligned} \tag{5}$$

With this choice of reference state, the states $|\chi^{(+)}\rangle$ and $\chi^{(-)}\rangle$ are single-particle and single-antiparticle states, respectively. In the second-quantized representation, the corresponding annihilation operators a_q and b_q satisfy the relations

$$\begin{aligned}&a_q|0\rangle=b_q|0\rangle=0\ ,\\&\{a_q,a_p^\dagger\}=\{b_q,b_p^\dagger\}=\delta_{q,p}\ .\end{aligned} \tag{6}$$

All other combinations of anticommutators of the operators a and b that do not appear in (6) are zero.

(iii) We assume the dynamics governing the time evolution of the states in (2) is unitary; that is,

$$|\Phi(t)\rangle=K(t,-\infty)|0\rangle\ , \tag{7}$$

where $KK^\dagger=K^\dagger K=1$. There are several important consequences of these assumptions. Equations (4) and (7) guarantee that the state Φ is at all times a representation of a single Slater determinant, and equations of motion can be cast into the form

$$H(x)K(t,t')=i\partial_t K(t,t')\ , \tag{8}$$

where

$$\begin{aligned}&H(x)=H_0(x)+V(x)\ ,\\&H_0(x)=-i\boldsymbol{\alpha}\cdot\boldsymbol{\nabla}+\gamma_0 m\ ,\\&V(x)=-\boldsymbol{\alpha}\cdot\mathbf{A}(x)+A_0(x)\ .\end{aligned} \tag{9}$$

With the above noted assumptions, all orders of processes can be obtained from the solutions to (8). In particular, those solutions which are perturbative in A^μ can be expressed as the series

$$K(t,\infty)=K_0(t,-\infty)+(-i)\int_{-\infty}^{t}d\tau\,K_0(t,\tau)V(\tau)K_0(\tau,-\infty)$$
$$+(-i)^2\int_{-\infty}^{t}d\tau\int_{-\infty}^{\tau}d\tau'\,K_0(t,\tau)V(\tau)K_0(\tau,\tau')V(\tau')K_0(\tau',-\infty)+\cdots\ , \tag{10}$$

where in (10), the lowest-order term is simply

$$K_0(t,t')=\exp[-iH_0(t-t')]\ . \tag{11}$$

In Fig. 1 we illustrate and label coordinates associated with the relativistic collision between two heavy ions a and b. For definiteness, we assume that the velocities are along the z axis, and that the centers of the nuclei of charge Z are separated in the transverse direction by an impact parameter $\boldsymbol{\rho}$. We employ natural units defined by $\hbar=c=m=e=1$. Each nucleus is moving in the c.m. frame with a kinetic energy per nucleon E related in these units to the Lorentz factor γ by $\gamma=E+1$. In (1),

$$A^\mu=A^\mu(a)+A^\mu(b)\ , \tag{12}$$

where the nonzero components of the potential from nucleus a are, in momentum space,

$$A^0(a)=-8\pi^2Z\gamma^2\frac{\delta(q_0-\beta q_z)}{q_z^2+\gamma_\perp^2}\exp\left[i\mathbf{q}_\perp\cdot\frac{\boldsymbol{\rho}}{2}\right]\ ,$$
$$A^z(a)=\beta A^0(a)\ . \tag{13}$$

The potentials from nucleus b can be easily obtained from (13) by the substitutions

$$\boldsymbol{\rho}\to-\boldsymbol{\rho},\quad \beta\to-\beta\ .$$

The semiclassical approximations that lead to the equations of motion, (8)–(10), also lead to a semiclassical approximation for the total inclusive production cross sections.[37] The two reactions

$$a+b\to e^-+X,\quad a+b\to e^-+e^++X'\ , \tag{14}$$

have very different total cross section yields even though electron-number conservation is preserved by (8) and (9). Assuming that the heavy-ion motion can be localized along definite impact parameters, the total inclusive singles σ_s and pair σ_p cross sections can be written in terms of the multiplicity of produced electrons $\mathcal{N}_s(\boldsymbol{\rho})$ and $\mathcal{N}_p(\boldsymbol{\rho})$ as

$$\sigma_s=\int d^2\rho\,\mathcal{N}_s(\boldsymbol{\rho})\ ,$$
$$\sigma_p=\int d^2\rho\,\mathcal{N}_p(\boldsymbol{\rho})\ . \tag{15}$$

Note that in the strong field limit the multiplicity of electrons is not a probability, but represents the mean number of electrons produced out of the vacuum. Denoting the time-evolved vacuum state in the interaction picture as

$$S|0\rangle=\lim_{t\to\infty}K_0(0,t)K(t,-t)|0\rangle\ , \tag{16}$$

the singles multiplicity can be written as

$$\mathcal{N}_s=\sum_{k>0}\langle 0|S^\dagger{:}a_k^\dagger a_k{:}S|0\rangle$$
$$=\sum_{k>0}\sum_{q<0}|\langle\chi_x^{(+)}|S|\chi_q^{(-)}\rangle|^2\ , \tag{17}$$

where the summation over the states k is restricted to those not occupied in the Dirac sea and the summation over the states q is restricted to those occupied in the Dirac sea. The pair multiplicity corresponds to an entirely different measurement and possesses correlations that are not accessible from a series of single measurements:

$$\mathcal{N}_p=\sum_{k>0}\sum_{q<0}\langle 0|S^\dagger{:}a_k^\dagger a_k b_q^\dagger b_q{:}S|0\rangle$$
$$=\sum_{k>0}\sum_{q'<0}|\langle\chi_k^{(+)}|S|\chi_{q'}^{(-)}\rangle|^2$$
$$\times\sum_{k'>0}\sum_{q<0}|\langle\chi_q^{(-)}|S|\chi_{k'}^{(+)}\rangle|^2$$
$$+\sum_{k>0}\sum_{q<0}\left|\sum_{q'<0}\langle\chi_k^{(+)}|S|\chi_{q'}^{(-)}\rangle\langle\chi_{q'}^{(-)}|S|\chi_q^{(-)}\rangle\right|^2\ . \tag{18}$$

The present discussion is limited to production out of the vacuum, but is easily extended to cases where the initial lepton number is nonzero. It is instructive to note that, in the perturbative limit, if the interaction is of the order of ϵ, then the first term on the right-hand side of (18) is of the order of ϵ^4, while the second term is of the order ϵ^2. In this limit the pair multiplicity is the same as the singles multiplicity, and the inclusive pair cross section is, $\sigma_p\simeq\sigma$,

$$\sigma=\int d^2\rho\sum_{k>0}\sum_{q<0}|\langle\chi_k^{(+)}|S|\chi_q^{(-)}\rangle|^2\ . \tag{19}$$

We consider such solutions in the next section.

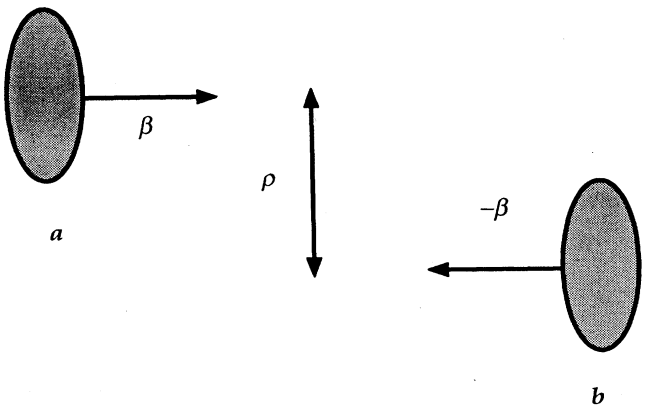

FIG. 1. Geometry and labeling convention for two colliding heavy ions.

III. TWO-PHOTON CROSS SECTIONS

In this section we develop perturbative solutions to (8) and (9) using time-dependent perturbation theory.[38] Our

method of time ordering the perturbation series and the corresponding rules for diagrams is similar to the Feynman theory for electrodynamics;[39] however, we note that the interaction Hamiltonian is constructed from the classical potentials (8) in the Lorentz gauge. In the c.m. frame, these functions have two nonzero components and are general functions of the energy-momentum transfer q. Except for the enumerating of the time orderings, the diagrams we calculate here are the same as those in the Feynman theory for the production of pairs from a time-dependent external field. The lowest-order diagrams which contribute to the amplitude in (19) are shown in Fig. 2. These terms correspond to the second-order terms in (10) and represent the summation over the possible time orderings, including the terms with crossed photon lines,[30]

$$\langle\chi_k^{(+)}|S|\chi_q^{(-)}\rangle=(-i)^2\int_{-\infty}^{\infty}d\tau\int_{-\infty}^{\tau}d\tau'\langle\chi_k^{(+)}|K_0(0,\infty)K_0(\infty,\tau)[V_a(\tau)K_0(\tau,\tau')V_b(\tau')+V_b(\tau)K_0(\tau,\tau')V_a(\tau')]$$
$$\times K_0(\tau',-\infty)K_0(-\infty,0)|\chi_q^{(-)}\rangle\ . \tag{20}$$

For purposes of clarity, it is convenient to identify and to discuss the contribution from each diagram in Fig. 2 separately; these are, respectively, S_{ab} and S_{ba}, with

$$S=S_{ab}+S_{ba}\ . \tag{21}$$

Although S is completely regular, most approximations introduced to simplify the calculation of (20), e.g., the equivalent photon method,[20–22,26,27] also introduce singularities; we shall see that this is quite unnecessary. Using completeness (5), the reduction of the time ordering is, in general,

$$\langle\chi_k^{(+)}|S_{ab}|\chi_q^{(-)}\rangle=i\int_{-\infty}^{\infty}\frac{d\omega}{2\pi}\sum_p\sum_s(E_p^{(s)}-\omega-i\eta^+)^{-1}\langle\chi_k^{(+)}|V_a(\omega-E_k^{(+)})|\chi_p^{(s)}\rangle\langle\chi_p^{(s)}|V_b(E_q^{(-)}-\omega)|\chi_q^{(-)}\rangle\ . \tag{22}$$

Energy-momentum conservation prevents the denominator in (22) from becoming zero and hereafter we shall choose η^+ as zero. For ultrarelativistic collisions, the potentials in (13) have an approximate factorization in terms of light-cone coordinates.[40,41] Although we shall not employ this procedure explicitly, it is worth remarking upon since it leads to a simple structure for (22) in terms of the invariants of the Lagrangian (1). The summation on the states of H_0 in (22) is over spin and momentum:

$$\sum_p=\sum_{\sigma_p}\sum_{\mathbf{p}}\rightarrow\sum_{\sigma_p}\int\frac{d^3p}{(2\pi)^3}\ . \tag{23}$$

The momentum in intermediate states is composed of parts transverse and parallel to the motion of the heavy ions $\mathbf{p}=\mathbf{p}_\perp+\mathbf{p}_z$. The momenta parallel to the motion of the heavy ions and the frequency in (22) are fixed by momentum conservation:

$$p_z=\frac{E_q^{(-)}-E_k^{(+)}+\beta(k_z+q_z)}{2\beta}\ ,$$
$$\omega=\frac{E_k^{(+)}+E_q^{(-)}-\beta(k_z-q_z)}{2}\ . \tag{24}$$

The transverse momentum is not fixed by kinematics, but depends on the momentum carried in the fields. Thus, for fixed momentum and spin states, the transition matrix element in (22) can be written as

$$\langle\chi_k^{(+)}|S_{ab}|\chi_q^{(-)}\rangle$$
$$=\frac{i}{2\beta}\int\frac{d^2p_\perp}{(2\pi)^2}\exp\left\{i\left[\mathbf{p}_\perp-\left[\frac{\mathbf{k}_\perp+\mathbf{q}_\perp}{2}\right]\right]\cdot\boldsymbol{\rho}\right\}$$
$$\times F(\mathbf{k}_\perp-\mathbf{p}_\perp:\omega_a)F(\mathbf{p}_\perp-\mathbf{q}_\perp:\omega_b)\mathcal{T}_{kq}(\mathbf{p}_\perp:\beta)\ , \tag{25}$$

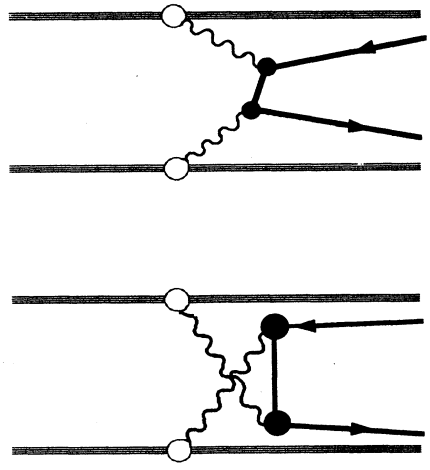

FIG. 2. Direct (a) and crossed (b) Feynman diagrams for pair production in a heavy-ion collision.

where ρ denotes the impact parameter and the function F is the scalar part of the field from each heavy ion. For point charge nuclei, F is given by

$$F(\mathbf{q}:\omega)=\frac{4\pi Z\gamma^2\beta^2}{\omega^2+\beta^2\gamma^2|\mathbf{q}|^2} . \tag{26}$$

Note that in (25) ω_a and ω_b are the frequencies associated with the fields of ions a and b, respectively,

$$\omega_a=\frac{E_q^{(-)}-E_k^{(+)}+\beta(q_z-k_z)}{2} ,$$
$$\omega_b=\frac{E_q^{(-)}-E_k^{(+)}-\beta(q_z-k_z)}{2} . \tag{27}$$

The function $\mathcal{T}$ explicitly depends on the velocity of the heavy ions β, on the transverse momentum $\mathbf{p}_\perp$, and on the states k,q: it is given by

$$\mathcal{T}_{kq}(\mathbf{p}_\perp:\beta)=\sum_s\sum_{\sigma_p}\left[E_p^{(s)}-\left[\frac{E_k^{(+)}+E_q^{(-)}}{2}+\beta\left[\frac{k_z-q_z}{2}\right]\right]\right]^{-1}$$
$$\times\langle u_{\sigma_k}^{(+)}|(1-\beta\alpha_z)|u_{\sigma_p}^{(s)}\rangle$$
$$\times\langle u_{\sigma_p}^{(s)}|(1+\beta\alpha_z)|u_{\sigma_q}^{(-)}\rangle , \tag{28}$$

where $u_\sigma^{(s)}$ is the spinor part of the states $\chi^{(s)}$. The longitudinal momentum implicit in (28), p_z, is determined by (24). Finally, we note that with the expression for the S matrix (25), the integration on the impact parameter for the pair cross section can be explicitly evaluated. Including both the direct and crossed photon contributions yields the result

$$\sigma=\frac{1}{4\beta^2}\sum_{\sigma_k\sigma_q}\int\frac{d^3k\,d^3q\,d^2p_\perp}{(2\pi)^8}\times|\mathcal{A}^{(+)}(k,q:\mathbf{p}_\perp)+\mathcal{A}^{(-)}(k,q:\mathbf{k}_\perp+\mathbf{q}_\perp-\mathbf{p}_\perp)|^2 , \tag{29}$$

where,

$$\mathcal{A}^{(+)}(k,q:\mathbf{p}_\perp)=F(\mathbf{k}_\perp-\mathbf{p}_\perp:\omega_a)F(\mathbf{p}_\perp-\mathbf{q}_\perp:\omega_b)\mathcal{T}_{kq}(\mathbf{p}_\perp:+\beta) ,$$
$$\mathcal{A}^{(-)}(k,q:\mathbf{p}_\perp)=F(\mathbf{k}_\perp-\mathbf{p}_\perp:\omega_b)F(\mathbf{p}_\perp-\mathbf{q}_\perp:\omega_a)\mathcal{T}_{kq}(\mathbf{p}_\perp:-\beta) . \tag{30}$$

A. Analytic reductions

Before evaluating the pair cross section (29) exactly by numerical means, we shall explore some approximate analytic reductions. Our objective is threefold. We wish to understand certain features exhibited by the exact results, in particular their rigorous gauge invariance, and their asymptotic behavior. In view of the diverse approximations existing in the literature under the heading of the "virtual-photon method," we feel it is useful to derive some tractable forms from (30) with as few approximations as possible, and these clearly stated. Finally, analytic formulas are a convenient means to interpolate exact results, e.g., multiply differential cross sections.

We shall adopt the view that these approximations are justified, insofar as they agree with the exact results. For completeness, we shall also rederive the virtual-photon method.[27]

The amplitude $\mathcal{T}$, defined in (28), relates the intermediate-photon lines to the outgoing-fermion lines. It can be reduced by summing over the intermediate spinor indices s,σ_p, with the aid of projection operators to find

$$\mathcal{T}_{kq}(\mathbf{p}_\perp:\beta)=\left\langle u_{\sigma_k}^{(+)}\middle|(1-\beta\alpha_z)\frac{H_0(\mathbf{p})+\omega}{H_0(\mathbf{p})^2-\omega^2}(1+\beta\alpha_z)\middle|u_{\sigma_q}^{(-)}\right\rangle , \tag{31}$$

where

$$H_0(\mathbf{p})=H_\perp(\mathbf{p}_\perp)+p_z\alpha_z ,$$
$$H_\perp(\mathbf{p}_\perp)+\boldsymbol{\alpha}_\perp\cdot\mathbf{p}_\perp+\gamma_0 , \tag{32}$$

and where (ω,p_z) depend on β, as in (24).

We shall consistently assume that $\gamma\gg1$, so that $\gamma\simeq3$ is the lowest energy of interest. Then all transverse momenta can be assumed much smaller than any longitudinal momenta, for the range contributing to the cross section. It is a consequence of the Lorentz transformation that $p_\perp\simeq mc$, while $p_z\simeq\gamma mc$.

All approximations to (29) seek to integrate out the transverse momentum $(\mathbf{k}_\perp,\mathbf{p}_\perp,\mathbf{q}_\perp)$, resulting in an expression of the form

$$\sigma=\int dk_z dq_z d^2K\,\Phi(\omega_a)\Phi(\omega_b)\sigma_{\gamma\gamma}(\omega_a,\omega_b:m_\perp) , \tag{33}$$

where

$$\mathbf{K}=\tfrac{1}{2}(\mathbf{k}_\perp+\mathbf{q}_\perp) \tag{34}$$

is the transverse momentum of the pair, and where

$$m_\perp=(1+\mathbf{K}^2)^{1/2} \tag{35}$$

is the transverse mass. To derive (33) from (29) and (30), the form factors (26) are integrated over the transverse momentum to obtain "photon fluxes," e.g.,

$$\Phi(\omega)=\frac{1}{(2\pi)^3\beta\omega}\int d^2\lambda_\perp\lambda_\perp^2|F(\boldsymbol{\lambda}_\perp:\omega)|^2 . \tag{36}$$

If the momentum is cut off at $\lambda_\perp\simeq m_\perp$,

$$\Phi(\omega)=\frac{2Z^2}{\beta\omega}\mathcal{P}\left[\frac{\beta\gamma m_\perp}{\omega}\right] . \tag{37}$$

The function $\mathcal{P}(x)$ is defined in Appendix A; for large x,

$\mathcal{P}(x)\sim\ln(x)$. The remaining factor in (33) is an effective two-photon cross section $\sigma_{\gamma\gamma}$ derived from $\mathcal{T}_{kq}$.

B. Two-peak approximation

The most obvious way to eliminate the transverse momenta from (29) is to observe that the form factors are strongly peaked about the point

$$\mathbf{k}_\perp,\mathbf{p}_\perp,\mathbf{q}_\perp\simeq\mathbf{K}\ . \tag{38}$$

If $\mathcal{T}$ is evaluated at this point, it vanishes as γ^{-4}. In Appendix A, we show that the leading term obtained by expanding in powers of $(\mathbf{p}_\perp-\mathbf{K})$ is

$$\mathcal{T}_{kq}^{\mathrm{TG}}(\mathbf{p}_\perp;\beta)\simeq\left\langle u_{\sigma_k}^{(+)}\left|\frac{\boldsymbol{\lambda}\cdot\boldsymbol{\alpha}}{\omega_a}\frac{H_0(\mathbf{p})+\omega}{H_0(\mathbf{p})^2-\omega^2}\frac{\boldsymbol{\mu}\cdot\boldsymbol{\alpha}}{\omega_b}\right|u_{\sigma_q}^{(-)}\right\rangle\ , \tag{39}$$

where $\boldsymbol{\lambda}=\mathbf{k}_\perp-\mathbf{p}_\perp$, $\boldsymbol{\mu}=\mathbf{q}_\perp-\mathbf{p}_\perp$. This form of the amplitude can be simply obtained by carrying out the perturbation expansion directly in the temporal gauge. In this case the interaction in the Lorentz gauge,

$$V_a^{\mathrm{LG}}(\boldsymbol{\lambda})=F(\boldsymbol{\lambda}:\omega_a)(1-\beta\alpha_z)\ , \tag{40}$$

is replaced by the corresponding interaction in the temporal gauge:

$$V_a^{\mathrm{TG}}(\boldsymbol{\lambda})=F(\boldsymbol{\lambda}:\omega_a)\left[-\frac{\alpha_z}{\beta\gamma^2}+\frac{\boldsymbol{\lambda}\cdot\boldsymbol{\alpha}_\perp}{\omega_a}\right]\ . \tag{41}$$

Note that (39) is obtained in the limit of very-high-energy collisions, where the longitudinal term α_z becomes negligible. The equivalence of the amplitudes in two different gauges is discussed in Appendix A and hinges entirely on cancellations between the terms $\mathcal{A}^{(+)}$ and $\mathcal{A}^{(-)}$ in (30), corresponding to the direct and crossed diagrams in Fig. 2.

If all frequencies and momenta in (39), except the leading powers of $\boldsymbol{\lambda}$ and $\boldsymbol{\mu}$, are evaluated at the point $\mathbf{p}_\perp=\mathbf{K}$, we immediately obtain from (29) an expression for the differential cross section of the form (33):

$$\frac{d^4\sigma}{dk_z dq_z d^2K}=\frac{8}{\pi^2\beta^4}(Z\alpha)^4\frac{\mathcal{P}(\beta\gamma m_\perp/\omega_a)\mathcal{P}(\beta\gamma m_\perp/\omega_b)}{[m_\perp^2E_k^{(+)}E_q^{(-)}(1+Z/\gamma^2)^2]^2}\times(\mathcal{W}_0^2+\mathcal{W}_1^2K^2)\ . \tag{42}$$

The rather complicated functions $\mathcal{W}_0$, $\mathcal{W}_1$, and Z of $(k_z,q_z,m_\perp)$ are defined in Appendix A. It is worth noting here that

$$Z\simeq|E_k^{(+)}E_q^{(-)}|/(\gamma m_\perp)^2\ , \tag{43}$$

so that the integrations over (k_z,q_z) cut off rapidly whenever $|k_z|,|q_z|\geq\gamma m_\perp$.

After integrating (42) over k_z and q_z, $d^2\sigma/d^2K$ decreases as $m_\perp^{-4}$. Thus, the above approximation leads to a finite total cross section without further assumptions. Each factor of $\mathcal{P}$ results in a contribution to the cross section which goes as $\ln(\gamma)$ asymptotically, but the integrations over k_z and q_z fall less rapidly than $\ln(\gamma)$; thus overall, (42) predicts $\sigma\sim\ln(\gamma)^2$.

We refer to (42) as the "two-peak approximation." The exact results suggest that it is valid for $\gamma\leq100$. The essence of the two-peak approximation is that most of the cross section comes from intermediate transverse momenta, $\mathbf{p}_\perp\simeq\mathbf{K}$. At this point, terms behaving as $(E_k^{(+)}-E_q^{(-)})^{-2}$ for large magnitudes of $E_k^{(+)}$ and $E_q^{(-)}$ cancel, removing a $\ln(\gamma)$ from the asymptotic formula.

C. Small-transverse-momentum approximation

For very large γ, say $\gamma\geq100$, values of $\mathbf{p}_\perp\neq\mathbf{K}$ begin to dominate the integration, so that a better approximation to (29) is to integrate first over $\mathbf{p}_\perp$, and then use (38) for $\mathbf{k}_\perp,\mathbf{q}_\perp$ to obtain a form similar to (42). This leads to an expression

$$\frac{d^4\sigma}{dk_z dq_z d^2K}=\frac{8}{\pi^2\beta^4}(Z\alpha)^4\frac{\mathcal{P}(\beta\gamma m_\perp/\omega_a)\mathcal{P}(\beta\gamma m_\perp/\omega_b)}{[m_\perp^2E_k^{(+)}E_q^{(-)}(1+Z/\gamma^2)^2]^2}\mathcal{W}_2^2\ . \tag{44}$$

The expression for $\mathcal{W}_2$ is given in Appendix A. Since $\mathcal{W}_2\sim(E_k^{(+)}-E_q^{(-)})$, (44) predicts, for large γ,

$$\alpha\simeq3.40(Z\alpha)^4\ln(\gamma)^3\ . \tag{45}$$

The coefficient here is slightly larger than the Weizsäcker-Williams value of $224/27\pi\simeq2.64$. We refer to (44) as the "small transverse-momentum approximation."

IV. RESULTS AND CONCLUSIONS

We shall present exact calculations of the second-order perturbation formula derived in Sec. III. The integrations in (29) were evaluated by Monte Carlo techniques to an accuracy of about 1%. Details of the numerical method are given in Appendix B. We note that extensive tests of the numerical procedures have been carried out, including calculations of the pair production starting from the two different gauges (40) and (41). Even though the diagrams in Fig. 2 are not individually gauge invariant, the sum is gauge invariant, which we have confirmed numerically. Our numerical results can be compared with a variety of approximate results, though we focus on the two-peak formula (42), which appears nearly to reproduce the exact results over a wide range of energies.

A. Total cross sections

In Fig. 3 we show the variation of the total cross section with energy for colliding beams of heavy ions. As previously stated, $\gamma-1$ is the beam kinetic energy per nucleon in units where the nucleon mass is 1. The cross section for producing an electron pair from ions of charges (Z_a,Z_b) is expressed in terms of the reduced cross section σ_0:

$$\sigma_0=\lambda^2Z_a^2Z_b^2\alpha^4\ , \tag{46}$$

where $\lambda=\hbar/mc$ is the reduced Compton wavelength of

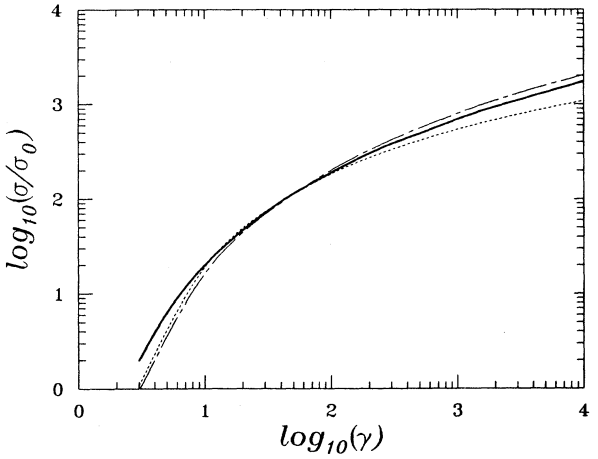

FIG. 3. Dependence of pair production cross section with energy. The ratio of the cross section to the reduced cross section defined by (46) is plotted vs γ. The three curves are solid line, exact numerical result; dashed line, two-peak approximation (42); long-short dashed line, small-momentum-transfer approximation (44).

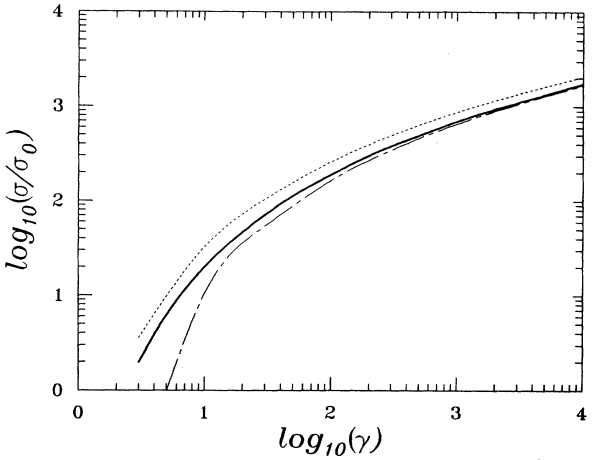

FIG. 4. Dependence of pair production cross section with energy. The ratio of the cross section to the reduced cross section defined by (46) is plotted vs γ. Solid line: exact numerical result; dashed line: equivalent-photon approximation (Ref. 20); long-short dashed line: modified Weizsäcker-Williams (Ref. 26).

the electron. For $Au+Au$, $\sigma_0=0.165Kb$. Our exact results are compared with the two-peak approximation (42), and the small-momentum-transfer approximation (44). Both reproduce the exact results to about 20% over the range of energies per nucleon between 3–300 GeV, which will be of most experimental interest in the near future.

For $\gamma>300$, terms of order $\ln(\gamma)^3$ begin to dominate. Indeed, the exact results can be fitted for all $\gamma>3$ by the formula

$$\sigma=C_\infty\sigma_0\frac{\ln(\gamma)^3}{1+0.4570Y+0.0222Y^2+\cdots}\ , \tag{47}$$

where

$$Y=\ln[1+(g_0/\gamma)^2]\ , \tag{48}$$

and the other fitted parameters are $C_\infty=2.19$ and $g_0=10^3$. The small-momentum-transfer approximation has a similar form with $C_\infty=3.40$. The two-peak result increases only as fast as $\ln(\gamma)^2$. As explained in Appendix A, this is due to the exact cancellation, at the peak of the Coulomb form factors, of terms which fall off inversely as the pair energy squared. For very large γ, contributions to the integrals from other values of the transverse momenta become more important.

Figure 4 compares the exact results with two currently quoted approximations. The dotted curve is the *equivalent-photon approximation* of Ref. 20, which is essentially a modern version of the Weizsäcker-Williams method with $C_\infty=224/27\pi\simeq2.64$. The dot-dashed curve is calculated from the formulas of Ref. 26, which attempt to refine the Weizsäcker-Williams result. It is correct for large γ, but appears to break down by as much as a factor of 10 for $\gamma\leq20$.

B. Singles distributions

Differential cross sections provide more detailed insights. Figures 5–9 systematically compare exact results with the two-peak approximation. Figures 5 and 6 present angle and momentum distributions in the laboratory for a fixed-target experiment at an energy per nucleon of 200 GeV. This is equivalent to a colliding beam experiment with $\gamma=10$. Heavy-ion beams of this energy are presently available at CERN. The differential cross section of the produced electron in terms of the laboratory momentum $\mathbf{k}$ is obtained from (29) by

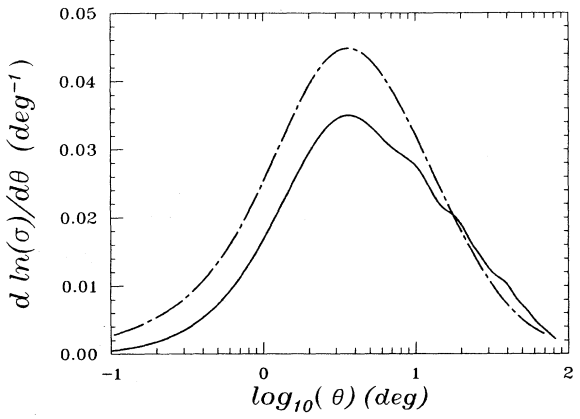

FIG. 5. Angular distribution in the laboratory for a fixed-target experiment at an energy per nucleon of 200 GeV, equivalent to a colliding beam experiment with $\gamma=10$. The normalized differential cross section (49) is plotted vs angle. Solid line: exact numerical result; long-short dashed line: two-peak approximation (42).

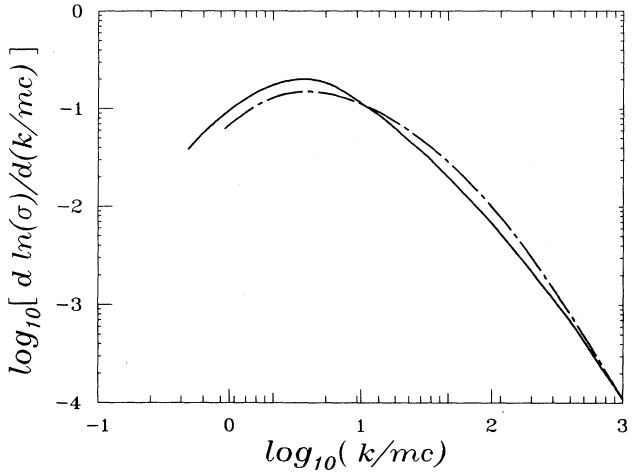

FIG. 6. Momentum distribution in the laboratory for a fixed-target experiment at an energy per nucleon of 200 GeV, equivalent to a colliding beam experiment with $\gamma=10$. The normalized differential cross section (49) is plotted vs momentum. Solid line: exact numerical result; long-short dashed line: two-peak approximation (42).

$$\sigma=\int_0^\infty dk\frac{d\sigma}{dk}=\int_0^{2\pi}d\theta\frac{d\sigma}{d\theta}\ , \tag{49}$$

where $\cos(\theta)=k_z/k$. The agreement between exact and approximate results, within 20%, is gratifying. The distributions computed in either way are consistent with a picture in which single leptons are ejected with $k_z\sim\gamma mc$ and $k_\perp\sim mc$; in this case, $\theta\sim 0.3°$ and $k\lesssim 200mc$.

C. Pair distributions

We next consider differential pair cross sections obtained from (29) in terms of the four-momentum of the pair

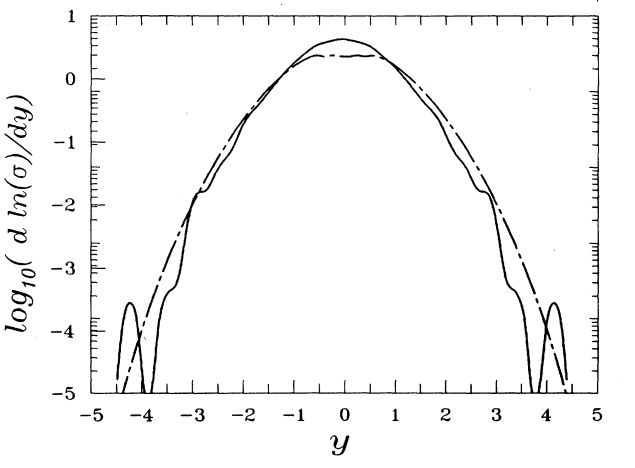

FIG. 7. Rapidity distribution for a collider experiment $\gamma=100$. The normalized differential cross section (56) is plotted vs Y. Solid line: exact numerical (Monte Carlo) result; long-short dashed line: two-peak approximation (42).

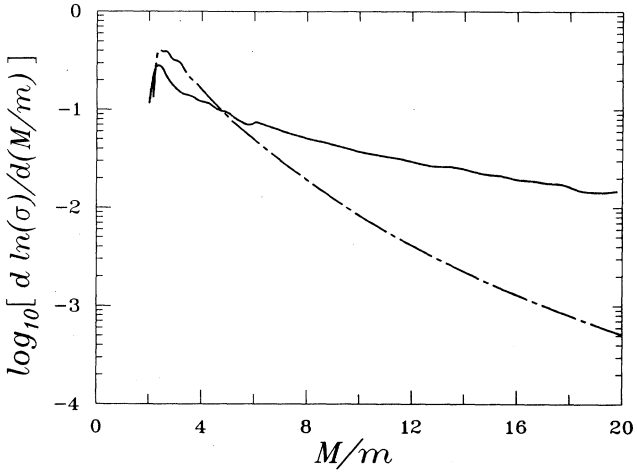

FIG. 8. Pair-mass distribution for a collider experiment at $\gamma=100$. The normalized differential cross section (56) is plotted vs M. Solid line: exact numerical (Monte Carlo) result; long-short dashed line: two-peak approximation (42).

$$P=k+q\ , \tag{50}$$

where k and q are the four-momenta of the electron and the positron, respectively. The three variables of interest are the rapidity

$$Y=\frac{1}{2}\ln\left[\frac{P_0+P_z}{P_0-P_z}\right]\ , \tag{51}$$

the invariant mass

$$M=(P_0^2-P_z^2-\mathbf{P}_\perp^2)^{1/2}\ , \tag{52}$$

and the transverse momentum

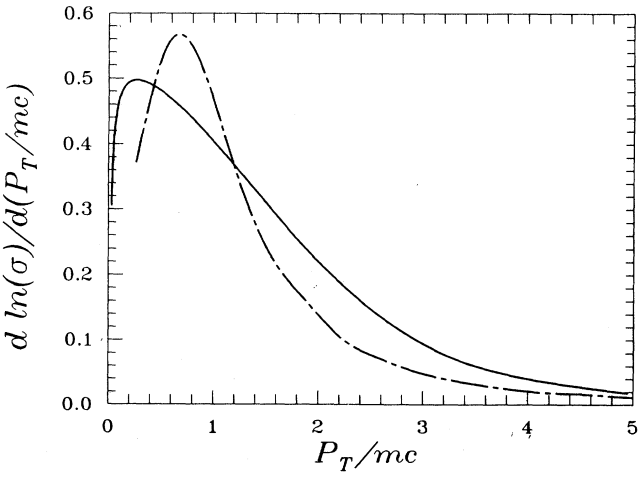

FIG. 9. Transverse-momentum distribution for a collider experiment at $\gamma=100$. The normalized differential cross section (56) is plotted vs P_T. Solid line: exact numerical (Monte Carlo) result; long-short dashed line: two-peak approximation (42).

$$P_T = |\mathbf{P}_\perp| \ . \tag{53}$$

In the Monte Carlo cross-section calculations, the distributions $d\sigma/dY$, $d\sigma/dP_T$, and $d\sigma/dM$ are obtained by accumulating the generated events into bins having the appropriate values of Y, P_T, and M. In the two-peak approximation, (42) is transformed using the relations

$$Y = \tfrac{1}{2}\ln(\omega_a/\omega_b), \quad M = (\omega_a\omega_b)^{1/2}, \quad P_T = 2K \ , \tag{54}$$

which are valid for small-transverse momenta, $K \ll |k_z|, |q_z|$, and the Jacobian

$$\frac{\partial(k_z,q_z)}{\partial(Y,M)} = \frac{4M}{(k_z/E_k^{(+)}) - (q_z/E_q^{(-)})} \ . \tag{55}$$

With these relations, it is straightforward to transform (42) numerically into the required form

$$\frac{d^3\sigma}{dY\,dM^2dP_T^2} = \frac{4}{\pi^2\beta^4}(Z\alpha)^4 \frac{\mathcal{P}(\beta\gamma m_\perp/\omega_a)\mathcal{P}(\beta\gamma m_\perp/\omega_b)}{[m_\perp^2 E_k^{(+)}E_q^{(-)}(1+Z/\gamma^2)^2]^2} \times \frac{(\mathcal{W}_0^2 + \mathcal{W}_1^2 P_T^2/4)}{(k_z/E_k^{(+)}) - (q_z/E_q^{(-)})} \ . \tag{56}$$

Figures 7–9 compare the Monte Carlo and two-peak results for the Y, M, and P_T distributions, respectively. In each case $\gamma = 100$, corresponding to the proposed RHIC facility at Brookhaven. Again the agreement is excellent, except possibly at large values of M (> 10).

Very long Monte Carlo runs having more than 10^7 points, were needed to accumulate good statistics in the singly differential cross sections plotted in Figs. 5–9. Some degree of fluctuation is still visible. However, the two-peak approximation appears sufficiently reliable that we have used it to predict doubly differential cross sections presented by means of contour plots in the planes (Y,P_T), (Y,M), and (M,P_T). The (Y,P_T) plot in Fig. 10 clearly shows how the pair production is strongly peaked along the beam axis in the forward and backward directions. Figures 11 and 12 demonstrate the strong correlation between M and P_T, such that M is concentrated around $M \sim 2P_T$. The foregoing results of Figs. 10–12 are in quantitative accord with our earlier calculations using a coherent field model.[14,32]

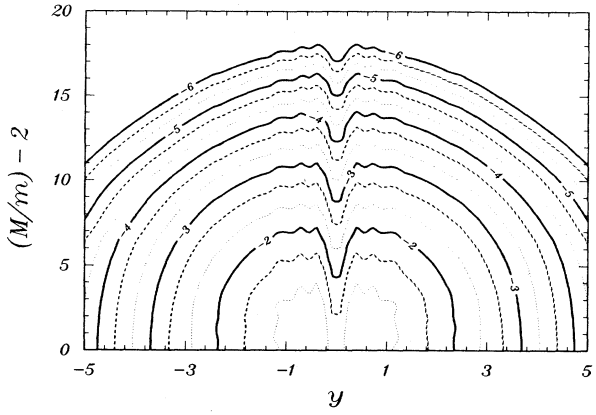

FIG. 11. Doubly differential cross sections: contours in the (Y,M) plane for a collider experiment at $\gamma = 100$ calculated from the two-peak approximation (42).

The formalism and calculations presented in this paper set the stage for further developments, in which we shall incorporate elastic and inelastic form factors for the nucleus and its constituents, and thus predict the production of heavy leptons, electroweak bosons, pions, etc. These processes can be evaluated at the two-photon level, either by exact numerical means, or in well-defined approximation schemes.

We further propose to use our results as a means of going beyond perturbation theory. At least three reasons can be advanced for believing that low-order perturbation theory gives an incomplete description of pair production in heavy-ion collisions. The supposedly small parameter $Z\alpha$ is comparable with unity. The asymptotic $\ln(\gamma)^3$ dependence of two-photon theory cannot be correct. The reasons supporting this statement are very

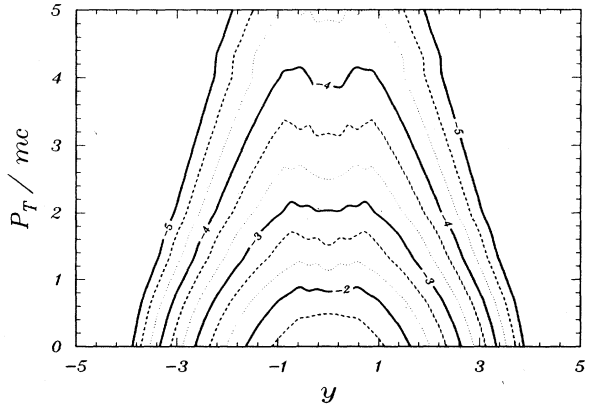

FIG. 10. Doubly differential cross sections: contours in the (Y,P_T) plane for a collider experiment at $\gamma = 100$ calculated from the two-peak approximation (42).

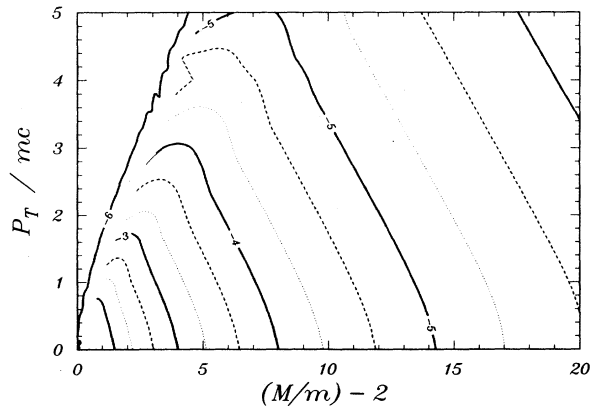

FIG. 12. Doubly differential cross sections: contours in the (M,P_T) plane for a collider experiment at $\gamma = 100$ calculated from the two-peak approximation (42).

simple, though they are rarely discussed. The Froissart cross-section bound[31] is believed to hold for electromagnetic, as well as for all other processes. This imposes a limit on the pair cross section at high energies: namely,

$$\sigma < \text{const} \times \ln(\gamma)^2 \ . \tag{57}$$

Finally, in higher orders, the N-photon contribution to the cross section $\sim \ln(\gamma)^{N+1}$ at least, demonstrating that the perturbation series should be resummed.

Nonetheless, we believe that the second-order perturbation results can be used heuristically to derive effective Lagrangians which can be solved nonperturbatively. This program will be pursued in future papers.

ACKNOWLEDGMENTS

This research was sponsored by the Division of Chemical Sciences, Office of Basic Energy Sciences, and by the Division of Nuclear Physics of the U.S. Department of Energy under Contract No. DE-AC05-84OR21400 with Martin Marietta Energy Systems, Inc.

APPENDIX A: APPROXIMATE ANALYTIC REDUCTIONS

The approximation leading to (42) can easily be visualized by an expansion process which takes (29) into the temporal gauge. We evaluate (29) by expanding in the momentum-transfer variables

$$\boldsymbol{\lambda}=\mathbf{k}_\perp-\mathbf{p}_\perp, \quad \boldsymbol{\mu}=\mathbf{q}_\perp-\mathbf{p}_\perp, \quad \boldsymbol{\tau}=(\boldsymbol{\lambda}+\boldsymbol{\mu})/2 \ , \tag{A1}$$

around the point $(\boldsymbol{\lambda},\boldsymbol{\mu})=0$ for which $\mathbf{k}_\perp=\mathbf{q}_\perp=\mathbf{K}$. Recall that $\mathbf{K}$ is defined in (34) as $\mathbf{K}=\frac{1}{2}(\mathbf{k}_\perp+\mathbf{q}_\perp)$. Thus we recast (29) in the form

$$\frac{d^4\sigma}{dk_z dq_z d^2K}=\frac{1}{4\beta^2}\int \frac{d^2\lambda d^2\mu}{(2\pi)^8}|F(\boldsymbol{\lambda}:\omega_a)F(\boldsymbol{\mu}:\omega_b)|^2 \times|\mathcal{T}_{kq}(\mathbf{K}-\boldsymbol{\tau}:\beta) +\mathcal{T}_{kq}(\mathbf{K}+\boldsymbol{\tau}:-\beta)|^2 \ , \tag{A2}$$

where

$$\mathcal{T}_{kq}(\mathbf{p}_\perp:\beta)=\left\langle u^{(+)}_{\sigma_k}\left|\theta^{(-)}\frac{H_0(\mathbf{p})+\omega}{H_0(\mathbf{p})^2+\omega^2}\theta^{(+)}\right|u^{(-)}_{\sigma_q}\right\rangle \ , \tag{A3}$$

and

$$\mathbf{p}=\mathbf{p}_\perp+\mathbf{e}_z p_z, \quad \theta^{(\pm)}=1\pm\beta\alpha_z \ . \tag{A4}$$

We introduce the abbreviations

$$Y_k=E_k^{(+)}+k_z, \quad Y_q=E_q^{(-)}+q_z \ , \tag{A5}$$

and repeatedly use the relation (24), which explicitly depends on the heavy-ion velocity β. All these quantities are functions of a single transverse mass $m_\perp^2=1+\mathbf{K}^2$. Making use of the foregoing, we can express all the amplitudes in terms of Y_k, Y_q, $m_\perp$, and γ. We shall frequently need the denominator

$$\mathcal{D}(\mathbf{p}_\perp:\beta)=H_0(\mathbf{p}_\perp,p_z)^2-\omega^2 \ , \tag{A6}$$

where H_0 is the free Dirac Hamiltonian defined in (33), and which depends on β through p_z and ω. In (A6), $\mathbf{p}_\perp$ is an independent variable which is evaluated at $\mathbf{p}_\perp=\mathbf{K}$:

$$1/\mathcal{D}(\mathbf{K}:+\beta)=Y_k/\mathcal{D}_0, \quad 1/\mathcal{D}(\mathbf{K}:-\beta)=-Y_q/\mathcal{D}_0 \ , \tag{A7}$$

where we employ the notation

$$\mathcal{D}_0=m_\perp^2(Y_k-Y_q)(1+Z/\gamma^2) \ , \qquad Z=-\frac{1}{4}\left[\frac{Y_kY_q}{m_\perp^2}+\frac{m_\perp^2}{Y_kY_q}\right] \ . \tag{A8}$$

We also make use of the identity

$$\omega_a\omega_b=\frac{m_\perp^2(Y_k-Y_q)^2}{-4Y_kY_q}(1+Z/\gamma^2) \ . \tag{A9}$$

Our results can now be established concisely with the aid of the relations

$$\theta^{(-)}(\omega+p_z\alpha_3)\theta^{(+)}=(\omega+p_z\alpha_3)/\gamma^2 \ , \qquad H_\perp(\mathbf{p}_\perp)\theta^{(+)}=\theta^{(-)}H_\perp(\mathbf{p}_\perp) \ , \qquad \sum_{j=\pm}\frac{\omega(j\beta)+p_z(j\beta)\alpha_z}{\mathcal{D}(j\beta)}=O(1/\gamma^4) \ . \tag{A10}$$

These follow from (A7) after some calculation. We shall transform (A3) by expanding the amplitude $\mathcal{T}_{kq}(\mathbf{p}_\perp:\beta)$ as a series in $H_0(\mathbf{p})-\omega$, resulting in

$$\mathcal{T}_{kq}(\mathbf{K}\pm\boldsymbol{\tau}:\beta)=\langle u^{(+)}_{\sigma_k}|\theta^{(-)}\Lambda(\mathbf{K}:\beta)^{-1}[1\pm\boldsymbol{\alpha}_\perp\tau\Lambda(\mathbf{K}:\beta)^{-1} +\boldsymbol{\alpha}_\perp\cdot\boldsymbol{\tau}\Lambda(\mathbf{K}:\beta)^{-1}\boldsymbol{\alpha}_\perp\cdot\boldsymbol{\tau}\Lambda(\mathbf{K}:\beta)^{-1}+\cdots] \times\theta^{(+)}|u^{(-)}_{\sigma_q}\rangle \ . \tag{A11}$$

By applying the relations (A11), it is easy to show that the first two terms cancel as far as $O(1/\gamma^4)$ when $\mathcal{T}_{kq}(\mathbf{K}+\boldsymbol{\tau}:\beta)$ is added to $\mathcal{T}_{kq}(\mathbf{K}-\boldsymbol{\tau}:-\beta)$. This leaves the third term which can be recast in the form of (39), using (A11) together with (A7) and (A9):

$$\mathcal{T}_{kq}(\mathbf{K}:\beta)+\mathcal{T}_{kq}(\mathbf{K}:-\beta) \simeq\left\langle u^{(+)}_{\sigma_k}\left|\frac{\boldsymbol{\lambda}\cdot\boldsymbol{\alpha}_\perp}{\omega_a}\frac{1}{\Lambda(\mathbf{K}:\beta)}\frac{\boldsymbol{\mu}\cdot\boldsymbol{\alpha}_\perp}{\omega_b}\right|u^{(-)}_{\sigma_q}\right\rangle \ . \tag{A12}$$

The denominator appearing in (A11) and (A12) is given by

$$\Lambda(\mathbf{p}_\perp:\beta)=H_\perp(\mathbf{p}_\perp)+p_z\alpha_z-\omega \ . \tag{A13}$$

Thus we observe that the leading term in the two-photon amplitude in the two-peak approximation is simply the amplitude in the temporal gauge. Apart from the explicitly displayed bilinear dependence on $\boldsymbol{\lambda}$ and $\boldsymbol{\mu}$, all quantities in (A12) are evaluated at the double peak, $(\boldsymbol{\lambda},\boldsymbol{\mu})=0$, or equivalently, $\mathbf{k}_\perp=\mathbf{q}_\perp=\mathbf{p}_\perp=\mathbf{K}$.

From (39), we can write the two-photon amplitude entering (29) in the form

$$\mathcal{T}_{kq}(\mathbf{K}:\beta)+\mathcal{T}_{kq}(\mathbf{K}:-\beta) \simeq\frac{1}{\omega_a\omega_b\mathcal{D}_0}\langle u^{(+)}_{\sigma_k}|\boldsymbol{\lambda}\cdot\boldsymbol{\alpha}_\perp H_\perp(\mathbf{K})\boldsymbol{\mu}\cdot\boldsymbol{\alpha}_\perp|u^{(-)}_{\sigma_q}\rangle \ . \tag{A14}$$

Again, use has been made of (A11) and (A7). Evaluating the spinors, we find that

$$\sum_{\sigma_k,\sigma_q} |\mathcal{T}_{kq}(\mathbf{K}:\beta)+\mathcal{T}_{kq}(\mathbf{K}:-\beta)|^2 \simeq \frac{1}{2}\left[\frac{\lambda\mu}{\omega_a\omega_b\mathcal{D}_0}\right]^2[(\eta_k-\eta_q)^2+\mathbf{K}^2(1-\eta_k\eta_q)^2], \tag{A15}$$

where $\eta_k=k_z/E_k^{(+)}$, $\eta_q=q_z/E_q^{(-)}$. Substituting (A15) into (A2) we can express the integrals over λ and μ in terms of the function

$$\mathcal{P}(x)=\frac{1}{2}\left[\ln(1+x^2)-\frac{x^2}{1+x^2}\right] \tag{A16}$$

introduced in (36) and (37). Employing the relations (A5)–(A9), we arrive at (42), with the following expressions for $\mathcal{W}_0$ and $\mathcal{W}_1$:

$$\mathcal{W}_0=\frac{Y_k+Y_q}{Y_k-Y_q},\quad \mathcal{W}_1=\frac{Y_k^2+Y_q^2}{(Y_k-Y_q)^2}. \tag{A17}$$

This is the *two-peak approximation* in which $|\mathcal{T}_{kq}(\mathbf{p}_\perp:\beta)|^2$ is evaluated at $\mathbf{p}_\perp=\mathbf{K}$. In contrast, the *small-momentum-transfer approximation* proceeds by first integrating $|\mathcal{T}_{kq}(\mathbf{p}_\perp)|^2$ over $\mathbf{p}_\perp$. Then the leading term is given by

$$\mathcal{T}_{kq}(\mathbf{p}_\perp:\beta)+\mathcal{T}_{kq}(\mathbf{p}_\perp:-\beta) \simeq \left\langle u_{\sigma_k}^{(+)}\left|\boldsymbol{\lambda}\cdot\boldsymbol{\alpha}_\perp\frac{\omega+p_z\alpha_z}{\omega_a\omega_b\mathcal{D}_0}\boldsymbol{\mu}\cdot\boldsymbol{\alpha}_\perp\right|u_{\sigma_q}^{(-)}\right\rangle, \tag{A18}$$

whence we calculate that

$$\sum_{\sigma_k,\sigma_q}\int d^2p_\perp|\mathcal{T}_{kq}(\mathbf{p}_\perp:\beta)+\mathcal{T}_{kq}(\mathbf{p}_\perp:-\beta)|^2 = \frac{\pi}{2}\frac{1}{|Y_kY_q|}\left[\frac{\lambda\mu m_\perp^2(m_\perp^2-Y_kY_q)}{\omega_a\omega_bE_k^{(+)}E_q^{(-)}}\right]^2. \tag{A19}$$

Functions of $\mathbf{p}_\perp$ other than $\mathcal{D}_0$ are evaluated at $\mathbf{p}_\perp=0$. The remaining integrations over $\boldsymbol{\lambda}\approx\mathbf{k}_\perp$ and $\boldsymbol{\mu}\approx\mathbf{q}_\perp$ are expressed in terms of $\mathcal{P}$, as before, leading to (43). The auxiliary function $\mathcal{W}_2$ is given by

$$\mathcal{W}_2=\frac{|Y_kY_q|^{1/2}(m_\perp^2-Y_kY_q)}{(Y_k-Y_q)^2}. \tag{A20}$$

APPENDIX B: MONTE CARLO INTEGRATION

The evaluation of (29) amounts to integrating a positive function over seven variables, since one integration can be removed by symmetry. We rewrite (29) in the form

$$\sigma=F_0\int f(x_1,x_2,\ldots,x_7)dx_1dx_2\cdots dx_7, \tag{B1}$$

where we denote these coordinates by the seven-dimensional vector

$$\mathbf{x}=\{\xi,\eta,K,\theta_\lambda,\phi_\lambda,\theta_\mu,\phi_\mu,\}, \tag{B2}$$

and the momentum variables by

$$\begin{pmatrix}k_z\\q_z\end{pmatrix}=\gamma e^\xi\begin{pmatrix}\cos\eta\\\sin\eta\end{pmatrix}, \tag{B3}$$

$$\begin{pmatrix}\lambda_x\\\lambda_y\end{pmatrix}=a_\lambda\tan\theta_\lambda\begin{pmatrix}\cos\phi_\lambda\\\sin\phi_\lambda\end{pmatrix}, \tag{B4}$$

$$\begin{pmatrix}\mu_x\\\mu_y\end{pmatrix}=a_\mu\tan\theta_\mu\begin{pmatrix}\cos\phi_\mu\\\sin\phi_\mu\end{pmatrix}. \tag{B5}$$

Adequate estimates of a_λ and a_μ are given by

$$a_\lambda(\xi,\eta,K)=\omega_a/\gamma,\quad a_\mu(\xi,\eta,K)=\omega_a/\gamma, \tag{B6}$$

evaluated at $\lambda=\mu=0$. The constant F_0 is so chosen that $f\le 1$. In the present case we have found it necessary to start with an estimate F_0, which is periodically improved by noting the largest value of f for varying numbers of Monte Carlo points.

The algorithm proceeds by making *throws* in an eight-dimensional space $\mathbf{y}=\{y_1,\ldots,y_8\}$, where $0<y_j<1$. We then calculate

$$x_8=f(y_1X_1,\ldots,y_7X_7), \tag{B7}$$

so that x_j lies in the range $0<x_j<X_j$. The *throw* is said to be *successful* if $x_8>y_8$. After T throws, let the number of successes be S. The cross section is given by

$$\sigma=F_0\frac{S}{T}\prod_{j=1}^{7}X_j, \tag{B8}$$

with a proportional error in σ/F_0 of

$$\Delta=\left[\frac{1}{S}+\frac{1}{T}\right]^{1/2}. \tag{B9}$$

Clearly, a good estimate of F_0 is desirable. We are able to compensate for the lack of *a priori* knowledge of F_0 by analyzing each throw for a set of F_0 in parallel. At the end of a run, the estimates of σ thereby obtained from

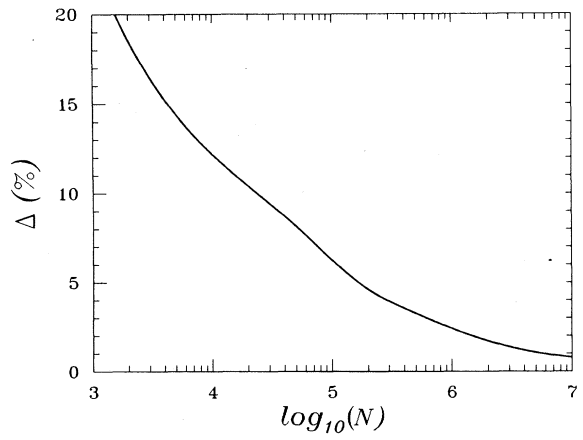

FIG. 13. Percentage error in Monte Carlo integration scheme, Δ, vs total number of points accumulated in a series of runs, N; see (B9).

(B8) were interpolated to the best value of F_0 inferred from the run itself. The improved value of F_0 was used in subsequent runs.

In Fig. 13 we display the error Δ as a function of the number of Monte Carlo points for a γ of 10^2. We observe a rapid and stable convergence of the sampling algorithm as described above. Typical success rates were $S/T \simeq 10^{-3}-10^{-4}$, whence $\Delta \simeq 30-100/T^{1/2}$.

[1]S. L. Wu, Phys. Rep. **107**, 59 (1984).
[2]F. Wilczek, Annu. Rev. Nucl. Part. Sci. **32**, 177 (1982).
[3]I. R. Kenyon, Rep. Prog. Phys. **45**, 1261 (1982).
[4]C. Rubbia, Rev. Mod. Phys. **57**, 699 (1985).
[5]R. H. Dalitz, Prog. Part. Nucl. Phys. **8**, 7 (1982).
[6]G. Domokos and J. Goldman, Phys. Rev. D **23**, 203 (1981); **28**, 123 (1983).
[7]K. Kajantie and H. I. Miettenen, Z. Phys. C **9**, 341 (1981); Z. Phys. **14**, 357 (1982).
[8]K. Kajantie, M. Kataja, L. McLerran, and P. V. Ruuskanen, Phys. Rev. D **34**, 811 (1986).
[9]K. Kajantie, J. Kapusta, L. McLerran, and A. Mekjian, Phys. Rev. D **34**, 2746 (1986).
[10]L. McLerran and T. Toimela, Phys. Rev. D **31**, 545 (1985).
[11]H. Gould, in *Atomic Theory Workshop on Relativistic and QED Effects in Heavy Atoms,* Gaithersburg, Maryland, 1985, edited by Hugh P. Kelly and Yong-Ki Kim (AIP Conf. Proc. No. 136) (AIP, New York, 1985).
[12]C. Bottcher and M. R. Strayer, in *Physics of Strong Fields,* proceedings of the International Advanced Course, Maratea, Italy, 1986, edited by W. Greiner (NATO ASI Ser. B. Vol. 153) (Plenum, New York, 1987), p. 629.
[13]E. Teller, in *Proceedings of the Ninth International Conference on the Application of Accelerators in Research and Industry,* edited by J. L. Duggan (North-Holland, New York, 1986).
[14]C. Bottcher and M. R. Strayer, in Proceedings of the Second Workshop on Experiments and Detectors for the RHIC, Berkeley, California, 1987 (unpublished).
[15]C. Bottcher and M. R. Strayer, Nucl. Instrum. Methods **B31**, 122 (1988).
[16]H. A. Bethe and W. Heitler, Proc. R. Soc. London **146**, 90 (1934).
[17]L. Landau and E. Lifshitz, Phys. Z. Sowjetunion **6**, 244 (1934).
[18]C. F. von Weizsäcker, Z. Phys. **88**, 612 (1934).
[19]E. J. Williams, K. Dan. Widensk, Selsk. Mat. Fys. Medd. **13**, 4 (1935).
[20]S. J. Brodsky, T. Kinoshita, and H. Terazawa, Phys. Rev. D **4**, 1532 (1971).
[21]F. E. Low, Phys. Rev. **120**, 582 (1960).
[22]R. H. Dalitz and D. R. Yennie, Phys. Rev. **105**, 1598 (1957).
[23]D. L. Olsen, B. L. Berman, D. E. Greiner, H. H. Heckman, P. J. Lindstrom, G. D. Westfall, and H. J. Crawford, Phys. Rev. C **24**, 1529 (1981).
[24]R. Anholt and H. Gould, in *Advances in Atomic and Molecular Physics,* edited by B. Bederson (Academic, New York, 1987).
[25]A. Goldberg, Nucl. Phys. **A240**, 636 (1984).
[26]G. Bauer and C. A. Bertulani, Phys. Rev. C **35**, 836 (1987).
[27]V. B. Berestetskii, E. M. Lifshitz, and L. P. Pitaevskii, *Quantum Electrodynamics,* 2nd ed., translated by J. B. Sykes and J. S. Bell (Pergamon, New York, 1979), p. 438.
[28]F. A. Berends, K. F. Gaemers, and R. Gastmans, Nucl. Phys. **B63**, 381 (1973).
[29]J. D. Bjorken and L. McLerran, Phys. Rev. D **31**, 63 (1985).
[30]F. Block and A. Nordsieck, Phys. Rev. **52**, 54 (1937).
[31]M. Froissart, Phys. Rev. **132**, 1053 (1961).
[32]C. Bottcher and M. R. Strayer, in *Frontiers of Heavy-Ion Physics,* edited by N. Cindro, W. Greiner, and R. Čaplar (World Scientific, Singapore, 1987), p. 471.
[33]J. D. Jackson, *Classical Electrodynamics* (Wiley, New York, 1962), p. 464.
[34]F. E. Close, *An Introduction to Quarks and Partons* (Academic, New York, 1979).
[35]K. Johnson, in *Brandeis Summer Institute in Theoretical Physics,* edited by S. Deser and K. W. Ford (Prentice-Hall, New York, 1964), Vol. 2, p. 1.
[36]C. Bottcher and M. R. Strayer, Ann. Phys. (N.Y.) **175**, 64 (1987).
[37]A. S. Umar, M. R. Strayer, D. J. Ernst, and K. R. S. Devi, Phys. Rev. C **30** 1934 (1984).
[38]M. Baranger and I. Zahed, Phys. Rev. C **29**, 1005 (1984).
[39]J. D. Bjorken and S. D. Drell, *Relativistic Quantum Fields* (McGraw-Hill, New York, 1965).
[40]J. D. Bjorken, J. B. Kogut, and D. F. Soper, Phys. Rev. D **3**, 1382 (1971).
[41]*Physics of Strong Fields,* edited by W. Greiner (Plenum, New York, 1987), Vol. 153, p. 1.